van der Waals-Induced Chromatic Shifts in Hydrogen-Bonded Two-Dimensional Porphyrin Arrays on Boron Nitride

Vladimir V. Korolkov,[†] Simon A. Svatek,[†] Alex Summerfield,[†] James Kerfoot,[†] Lixu Yang,[‡] Takashi Taniguchi,[§] Kenji Watanabe,[§] Neil R. Champness,[‡] Nicholas A. Besley,*[,‡] and Peter H. Beton*[,†]

[†]School of Physics & Astronomy and [‡]School of Chemistry, University of Nottingham, Nottingham NG7 2RD, U.K. and [§]The National Institute for Materials Science, Advanced Materials Laboratory, 1-1 Namiki, Tsukuba, Ibaraki 305-0044, Japan

ABSTRACT The fluorescence of a two-dimensional supramolecular network of 5,10,15,20-tetrakis(4-carboxylphenyl)porphyrin (TCPP) adsorbed on hexagonal boron nitride (hBN) is red-shifted due to, primarily, adsorbate−substrate van der Waals interactions. TCPP is deposited from solution on hBN and forms faceted islands with typical dimensions of 100 nm and either square or hexagonal symmetry. The molecular arrangement is stabilized by in-plane hydrogen bonding as determined by a combination of molecular-resolution atomic force microscopy performed under ambient conditions and density functional theory; a similar structure is observed on MoS_2 and graphite. The fluorescence spectra of submonolayers of TCPP on hBN are red-shifted by ∼30 nm due to the distortion of the molecule arising from van der Waals interactions, in agreement with time-dependent density functional theory calculations. Fluorescence intensity variations are observed due to coherent partial reflections at the hBN interface, implying that such hybrid structures have potential in photonic applications.

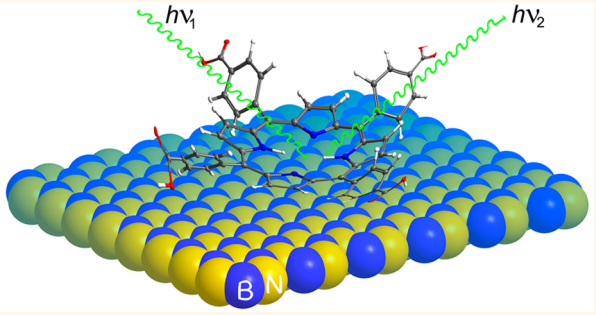

KEYWORDS: boron nitride · fluorescence · molybdenum disulfide · atomic force microscopy · porphyrin

There have been great advances over the past decade in the understanding of the interactions that stabilize the two-dimensional organization of organic molecules on surfaces.[1−4] This body of research provides a route to combine chemical functionality with spatial organization at the nanometer scale through the formation of templates and networks stabilized by hydrogen bonding, metal coordination, and/or covalent coupling.[5−16] Many of the advances in the field have arisen from studies of supramolecular arrangements on noble metal or highly oriented pyrolytic graphite (HOPG) surfaces, but it is clear that these substrates have some properties that are not compatible with investigations of the functional properties of the molecular arrays. In particular, the metallic nature of the substrates precludes subsequent investigations of the optical and electrical properties of self-assembled networks, limiting the potential to exploit the control of organization and functionality of the arrays. To extend these studies beyond the conventional choice of substrate, for example to include molecular organization on insulators, requires the use of atomic force microscopy (AFM), which has been used previously to acquire high-resolution images of 2D molecular and supramolecular organization under ultra-high-vacuum conditions,[17−22] but less widely[23−25] at atmospheric pressure due to the limitations of ambient AFM.

In this paper we combine a high-resolution AFM investigation of the supramolecular organization of the porphyrin derivative 5,10,15,20-tetrakis(4-carboxylphenyl)-porphyrin (TCPP) with a study of the fluorescence of the resulting molecular networks. The choice of TCPP is motivated, in part, by the role of porphyrins in naturally occurring light-harvesting complexes, as well as their potential as active materials in optoelectronic and sensing devices, and also since similar derivatives have been

* Address correspondence to nick.besley@nottingham.ac.uk; peter.beton@nottingham.ac.uk.

Received for review July 15, 2015 and accepted September 8, 2015.

Published online 10.1021/acsnano.5b04443

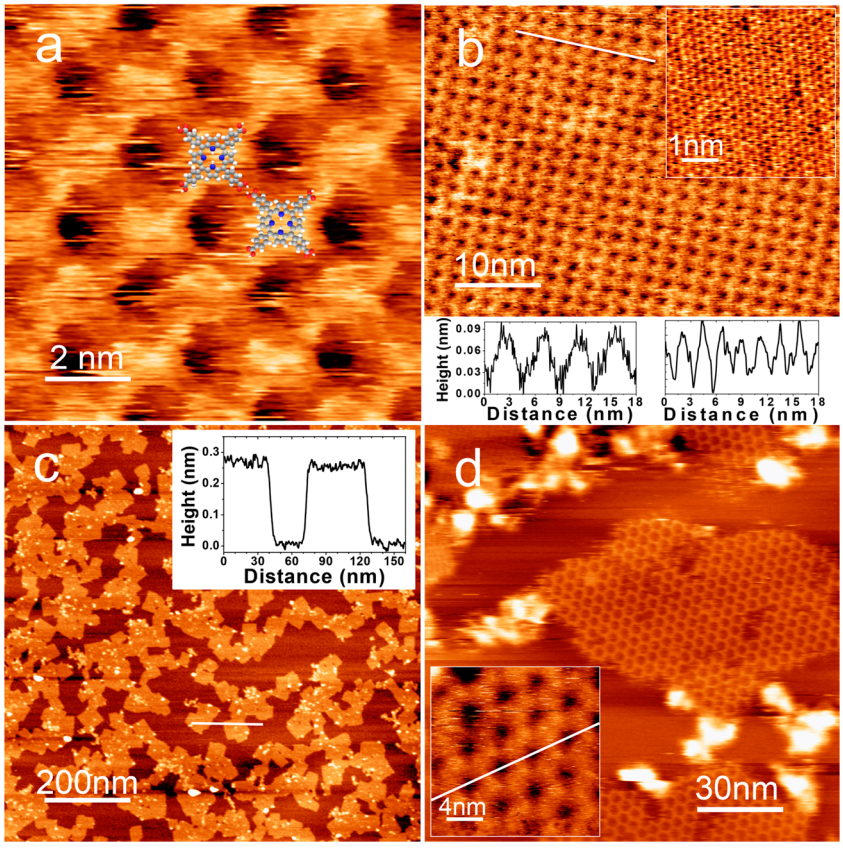

Figure 1. AFM images of TCPP adsorbed on hBN by immersion for 10 s in a 13 μM EtOH solution. (a) High-resolution scan of square TCPP phase; (b) larger area image showing square phase (upper inset) hBN lattice and (lower inset) height profiles of square and hexagonal arrays extracted from images along highlighted white lines in b (right) and d (left); (c) overview image of island morphology of TCPP; (d) hexagonal phase of TCPP; inset presents zoom-in showing additional detail and placement of the line along which profile in b is extracted. Images were acquired in (a) contact mode and (b–d) ac mode using an Asylum Cypher AFM.

widely studied previously on metallic surfaces.[26–29] The molecules are deposited from solution in an immersion process, and we have investigated the formation of networks on hexagonal boron nitride (hBN), an insulator, and, for comparison, the surfaces of highly oriented pyrolytic graphite and MoS_2. Using ambient AFM we are able to acquire images with subnanometer resolution, which are used to determine the lateral ordering of adsorbed molecules. Clear peaks are resolved in the fluorescence spectrum for submonolayer coverages of TCPP on hBN. We also observe a significant variation in the emission intensity, which depends on the thickness of the hBN layers due to coherent reflections at the upper and lower surfaces of the exfoliated flakes.

RESULTS

TCPP is deposited on all substrates (hBN, HOPG, and MoS_2) from solution (see Methods for details and cleaning procedures). High-resolution AFM images acquired under ambient conditions show TCPP molecules in two distinct phases on hBN, with, respectively, square (Figure 1a–c) and hexagonal (Figure 1d) symmetry (a structural model of TCPP is shown in Figure 2 and overlaid on Figure 1). In large-area images (Figure 1b,c) we see islands with typical dimensions of 50–100 nm. Inspection of the molecular arrangement within the two different types of islands reveals a square network assembly with a lattice constant of 2.22 $\pm$ 0.07 nm (Figure 1a and b) or a hexagonal arrangement with a period of 4.37 $\pm$ 0.07 nm (Figure 1d). We have found that the hexagonal arrangement is less stable to AFM imaging; this phase gradually disappears over a time scale of $\sim$1 day, whereas the square phase remains stable under atmospheric conditions for more than a week. It is also possible to resolve the hBN lattice as shown in the inset in Figure 1b.

The symmetry and period of these molecular arrangements are consistent with simple models based on junctions of two or three carboxylic acids for respectively the square and hexagonal phases, which in both cases are stabilized by hydrogen bonding. Molecular models for each phase are shown in Figure 2, and the expected dimensions and stabilization energies have in both cases been calculated using gas-phase density functional theory including dispersion corrections (DFT-D; see Supporting Information (SI) for more details). The periodicities derived from the

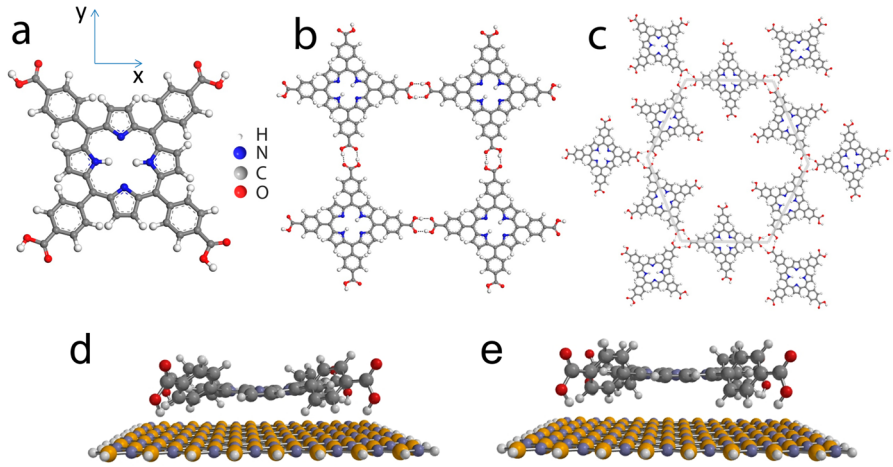

Figure 2. Structure of TCPP and calculated minimum-energy hydrogen-bonded and adsorbed structures. (a) Molecular structure and definition of axes; the *z*-axis is perpendicular to plane of the porphyrin; (b) square phase stabilized by hydrogen bonding between carboxylic acid dimers; (c) hexagonal phase stabilized by trimeric carboxylic acid vertices; (d and e) adsorbed molecule on hBN with and without dispersion forces, respectively.

calculated molecular separations are 2.31 nm (square) and 4.30 nm (hexagonal), very close to our measured values, while the binding energies per carboxylic acid junction are respectively 1.15 and 1.02 eV. This is equivalent to an energy per molecule within the square and hexagonal arrays of 2.30 and 0.68 eV, consistent with our observations that the square phase is more stable. Dispersion effects make a small contribution to the binding within the layer and contribute 0.13 eV/junction for both square and hexagonal lattices. The organizational motif forming the square phase is also present in the planes of molecules embedded in the bulk crystal structure of TCPP[30,31] in which the reported lateral lattice constant is 2.25 nm,[31] in agreement with our measured values. The trimer junction in the hexagonal phase is similar to that in the "flower" structure formed by trimesic acid and related molecules.[9,32]

In the topographic profile shown in Figure 1 the height of the molecular layers is measured to be 0.26 ± 0.015 nm. This height, and the close agreement between measured and calculated lateral dimensions, provides strong evidence that the molecules are adsorbed with the porphyrin macrocycle approximately parallel to the surface in an arrangement stabilized by hydrogen bonding.

The adsorption energy and geometry of TCPP on hBN has also been calculated using DFT-D. In these calculations the surface was modeled using a finite slab consisting of 80 boron atoms and 80 nitrogen atoms, and the edges were capped with hydrogen. The substrate−molecule interaction is dominated by van der Waals interactions; the calculated adsorption energy, including dispersion terms, is 4.06 eV/molecule, but in the absence of dispersion forces is much lower, 0.21 eV/molecule (see the SI). In fact the dispersion contribution to the overall binding energy of 4.06 eV is 5.28 eV, while there is an energetic cost due to the distortion of the molecular structure, which is computed to be 0.79 eV; the additional energy cost of 0.42 eV is likely due to the overlap of the electron density of the molecule and the surface. Consequently, the structure of the molecule absorbed on the surface represents a balance between maximizing the dispersion component at the cost of molecular deformation and repulsion between the electron densities. A comparison of the relaxed geometries of TCPP on hBN with and without dispersion (compare Figure 2d and e) shows that the macrocycle has a bowing distortion due to van der Waals interactions, which results in a reduction in the separation of the hBN and the porphyrin ring; this is equal to 0.337 nm (0.422 nm) with (without) dispersion.

The adsorption of a range of organic molecules such as phthalocyanines, perylene derivatives, and porphyrins on an hBN monolayer termination of a metal surface[33−35] has been reported previously; in these studies STM was used as an imaging modality since the molecules were sufficiently strongly coupled to the underlying metallic substrate. Deformation of porphyrin macrocycles has also been observed when related molecules are adsorbed on metal surfaces.[26,36,37]

The square arrangement of TCPP differs from those previously reported for molecular adsorption on HOPG by Lei *et al.*,[38] who found that scanning tunneling microscopy (STM) could be used to acquire images only when TCPP was coadsorbed with stearic acid. Under those conditions TCPP forms a more close-packed arrangement with a period of 1.83 nm. Yuan *et al.*[39] observed a similar closed-packed arrangement as well as two other phases on Au(111) in 0.01 M $HClO_4$ medium, one of which was attributed to a square network with an enclosed TCPP molecule.

In light of these differences we have also investigated the adsorption of TCPP layers, prepared using similar protocols, on HOPG and MoS_2. We observe the

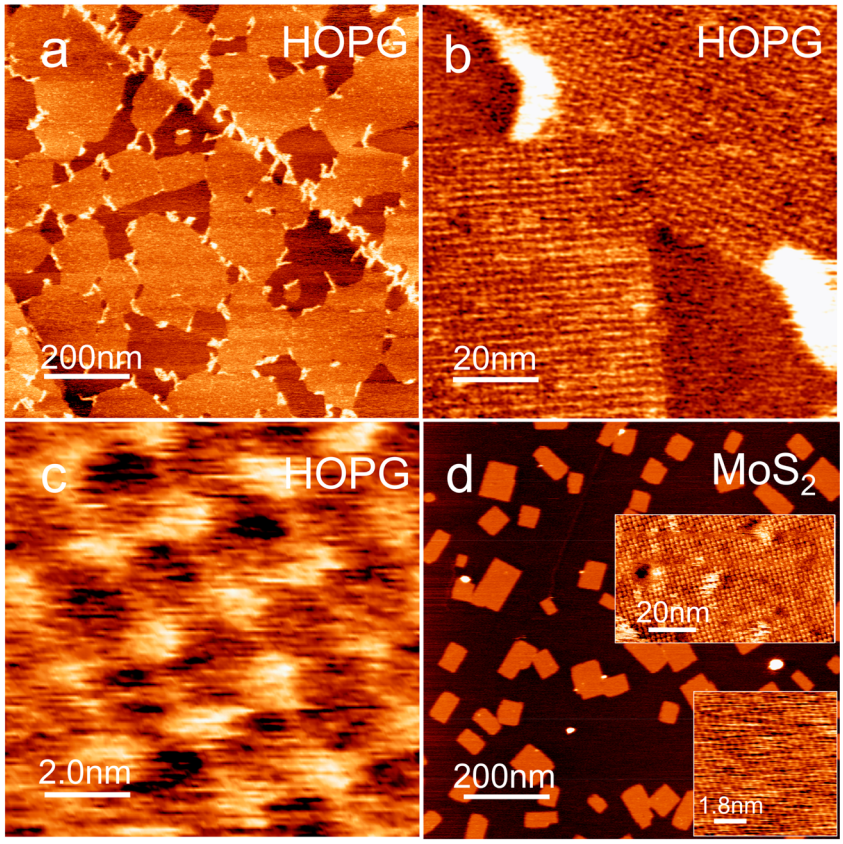

Figure 3. AFM images of TCPP adsorbed on HOPG (a−c) from a 140 μM DMF solution and MoS_2 (d) from a 13 μM EtOH solution. Adsorption time is ~1 s for all images. (a) Overview image showing islands of monolayers and crystallites; (b) two differently oriented phases of TCPP molecules; (c) high-resolution image showing square assembly; (d) single crystallites on MoS_2; (upper inset) zoom-in showing square arrangement of molecules; (lower inset) AFM image showing MoS_2 lattice. Images of TCPP on graphite were acquired in PeakForce tapping mode; the MoS_2 images were acquired using an Asylum Cypher in ac mode; the MoS_2 lattice was resolved in contact mode.

square network on HOPG, as shown in Figure 3, with the same period, 2.26 ± 0.05 nm, found for hBN. On HOPG we also observe rod-like structures of 30−50 nm in length and 1.5 ± 0.2 nm in height that are attributed to aggregates of nonplanar TCPP molecules. We have not been able to acquire images of this square phase on HOPG using STM, which we attribute to the compromise of the stability of the layers due to the STM tip as suggested previously by Lei *et al.*;[38] this suggests that AFM may have advantages for the imaging of weakly bound molecular monolayers. Images of TCPP networks have also been acquired following deposition on MoS_2, a layered semiconductor with a band gap of 1.23 eV that exhibits photovoltaic effects and electroluminescence.[40,41] The TCPP islands formed on MoS_2 (see Figure 3d) are very similar to the square phase discussed above for hBN and HOPG with a lattice constant of 2.24 ± 0.05 nm. We are also able to resolve the atomic lattice of the MoS_2 surface using AFM as shown in Figure 3d, inset. Thus, we observe the same square network structure for TCPP molecules on each of these surfaces.

We have investigated the fluorescence of TCPP adsorbed on hBN (no fluorescence was observed from TCPP adsorbed on either the HOPG or MoS_2 surfaces), and in Figure 4 we show spectra for TCPP in solution, adsorbed on hBN, and also on the SiO_2 exposed surface in the areas between exfoliated hBN flakes (an optical image of a typical area is shown in the inset in Figure 4). See Methods section for further experimental details.

In each spectrum the characteristic Q-band double peak is observed corresponding to the $Q_x(0,0)$ transition (close to 649 ± 1 nm (1.910 ± 0.003 eV) for the ethanolic TCPP solution) with a $Q_x(0,1)$ vibronic satellite at 716 ± 1 nm, in good agreement with previous studies.[42,43] These peaks are red-shifted on SiO_2 and hBN, with the $Q_x(0,0)$ peak occurring at 652 ± 1 nm (1.901 ± 0.003 eV) and 679 ± 2.5 nm (1.826 ± 0.007 eV), respectively. Thus, we observe an energy shift for TCPP on hBN of 0.084 ± 0.008 eV as compared with the ethanolic solution, but there is also a pronounced difference, 0.075 ± 0.008 eV, between TCPP adsorbed on hBN and SiO_2. There are several possible origins of this red-shift, and we consider the effects of intermolecular interactions and molecular deformation induced by molecule−surface interactions.

As discussed above, the porphyrin macrocycle of TCPP is deformed on adsorption on hBN, leading to a

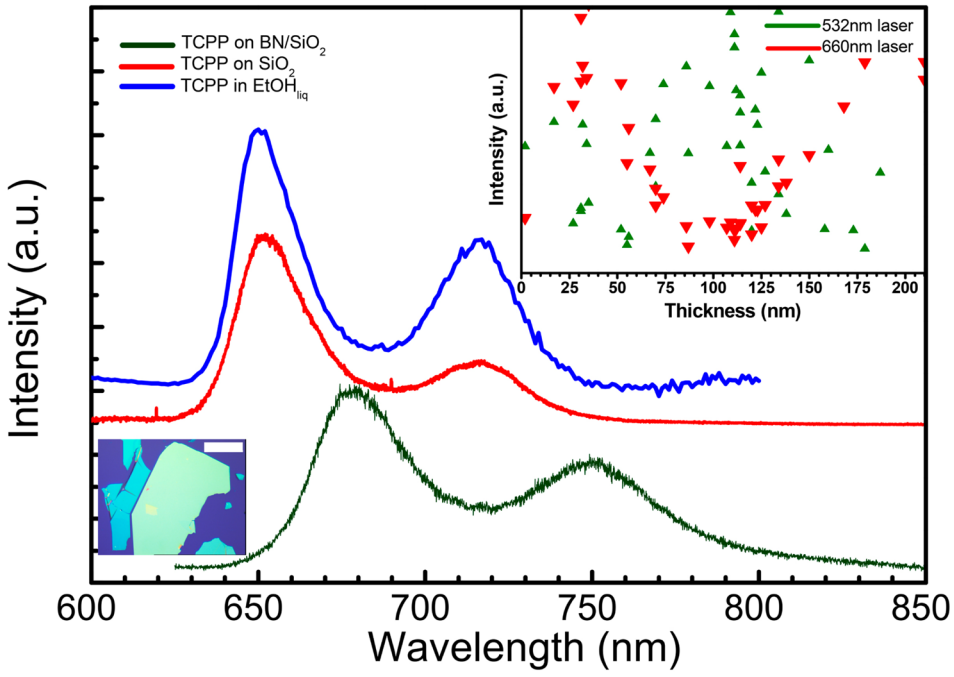

Figure 4. Normalized fluorescence emission spectra (excitation wavelength 532 nm) of TCPP molecules in an ethanolic solution (blue), assembled in the square phase on hBN (green), and on the SiO_2 surface between hBN flakes (red). Lower inset shows an optical (real color) image of hBN flakes; the dark blue is the bare SiO_2, while the green/blue flakes are the hBN. The scale bar is 50 μm. Upper inset: Variation of the intensity of the $Q_x(0,0)$ peak taken with the red and green laser for flakes with different thickness due to an interference effect.

bowed geometry. From our calculations it is clear that the bowing arises, at least in part, due to the presence of the aryl side groups, which cannot adopt a coplanar alignment with the porphyrin macrocycle due to steric considerations. Consequently the aryl side groups act analogously to small pedestals raising the plane of the macrocycle above the substrate surface. The resulting small gap allows flexing of the macrocycle due to van der Waals interactions with the surface, leading to the bowing effect. It has been shown that nonplanar conformations of a porphyrin macrocyle lead to red-shifts in the Soret and Q-band, and this has been attributed to a destabilization of the highest occupied molecular orbital[44] (HOMO). Another factor that is known to affect the fluorescence is the orientation of the aryl side groups with respect to the macrocycle,[42] which will also be affected by the presence of the surface. We have therefore used time-dependent density functional theory (TDDFT) to calculate fluorescence transition energies for both adsorbed and gas-phase molecules and to explore the origin of the observed spectral shifts. Note that TDDFT provides a more accurate description of the transition than a simple calculation of the HOMO−LUMO gap (LUMO is lowest unoccupied molecular orbital) since it includes the response of the electronic structure to the excited-state configuration.[45]

To calculate the fluorescence energy, the molecule is first optimized in the first excited state. This calculation is particularly demanding, and we are limited to a model system comprising a single molecule and the hBN monolayer (see Figure 2). The fluorescence energy of TCPP on hBN is calculated to be 1.99 eV (623 nm), which, for this type of calculation, represents very good agreement with the experimental values. The calculated shifts due to adsorption and surface interactions are derived by comparing the relevant transition in the gas phase and adsorbed molecules and summarized in Table 1 (the molecular orbitals associated with this transition are shown in the SI). The shift in fluorescence energy of adsorbed TCPP relative to the gas phase depends critically on dispersion forces (first row in Table 1). With dispersion forces included the calculated shift is −0.08 eV, but a much smaller positive shift of +0.02 eV is calculated in their absence. Thus, the

TABLE 1. Computed Structural Properties of the S_1 State of TCPP on hBN and Shift in Fluorescence Energy with Respect to the Gas Phase[a]

	without dispersion	with dispersion
transition energy shift (eV)	+0.02 (+0.02)	−0.08 (−0.05)
hBN-porphyrin spacing (nm)	0.435	0.339
transition dipole moment (Debye)	(3.35, −0.30, 0.01)	(3.86, −1.04, −0.08)
orientation of aryl groups (deg)	59.2	49.9
porphyrin HOMO energy (eV)	−5.55	−5.50
Pporphyrin LUMO energy (eV)	−3.04	−3.15

[a] Transition energies in parentheses correspond to an isolated TCPP molecule with the structure adopted on adsorption on hBN. The transition dipole moment vector lies in the plane of the porphyrin ring and is predominantly along the *x*-axis, *i.e.*, in the direction of the N−H groups at the center of the ring (the axes are defined in Figure 2).

adsorbate−substrate interaction both binds the molecule to the surface and also shifts its energy levels even for an unreactive surface such as hBN.

To deconvolve the influence of molecular distortion on the transition energy, as compared with a direct interaction with the hBN surface, we have also calculated the transition energy for the relaxed molecular geometries in the absence of the surface (included in brackets in the first row of Table 1). This shows that the largest contribution (−0.05 eV) to the calculated −0.08 eV shift arises from the intrinsic molecular distortion induced by van der Waals interactions; the additional contribution to the shift arises from interactions with the electron system in the model hBN surface.

The two most distinct changes in the structure observed on adsorption are the distortion of the porphyrin macrocycle and a flattening of the aryl side groups. Our results for the S_1 state (see Table 1) show a shift to higher energy of 0.05 eV of the HOMO on inclusion of dispersion, consistent with previous reports[44] of the destabilization of the HOMO for nonplanar conformations. Our calculations also show a decrease in energy of the LUMO, resulting in an overall red-shift. The orientation of the aryl groups, as measured by their average angle with respect to the plane of the porphyrin core, is about 9° smaller for the structure optimized with dispersion (see Table 1); aryl group rotation has been demonstrated in previous studies to give rise to a red-shift.[42]

We have also undertaken simulations of tetraphenylporphyrin (TPP), an analogous molecule in which the carboxylic acid groups are not present. These were performed to ensure that the calculations are not dominated by model-driven interactions between the carboxylic acids and the simulated hBN surface. Calculated structures of TPP on hBN also exhibit macrocycle distortion, with a shift in the fluorescence energy of −0.12 eV, similar to the value for TCPP (see the SI). The absorption and fluorescence energies for TCPP and TPP both on and off the surface are also included in the SI.

In addition to the shifts arising from changes in molecular conformation and the molecule−substrate interaction as discussed above, there are several other possible effects that might lead to a shift in the peak position. These are due to interactions between nearest neighbor TCPP molecules (our simulations treat an isolated molecule on hBN), which may be categorized as either resonant or nonresonant. The resonant shifts arise from the coupling of the transition dipole moment, μ_{TDM}, of neighboring molecules and have a typical energy scale of $\mu_{TDM}^2/4\pi\varepsilon_o r^3$ where r is the separation of dipoles.[46−49] Using the calculated value for $\mu_{TDM} \approx 4$ D (see Table 1) gives an energy scale of $\sim 1 \times 10^{-3}$ eV; taking into account the geometry and number of nearest neighbors leads to an estimate of a shift of $\sim 2 \times 10^{-3}$ eV, showing that this effect is small compared to the observed effect. This value is lower than that predicted by Vlaming *et al.*[50] for porphyrin chains due, in part, to the lower value of dipole moment used here. There is also a possible nonresonant shift due to intermolecular interactions, which we have attempted to capture by calculating the $S_1 \leftarrow S_0$ transition energy of a gas-phase TCPP hydrogen-bonded dimer (see the SI). The calculated shift is less than 10^{-3} eV, and, even noting that there are four nearest neighbors, this shows that nonresonant effects may be neglected; this result for a dimer also shows that the formation of hydrogen bonds does not have an intrinsic effect on the transition energy of TCPP. Overall the largest contribution to the calculated shift is due to variations in the electronic structure induced by the molecular deformation arising from the van der Waals molecule−substrate interaction, 0.08 eV.

We have so far neglected a possible chromatic shift between the gas phase of TCPP, for which experimental data are not available, and the solution phase, which serves as a reference for our measured data. However, we note that the fluorescence excitation spectrum of TPP (analogous to TCPP but with phenyl rather than carboxyphenyl side groups) in He droplets has been reported[51,52] to have a peak at ∼640 nm, which is red-shifted to 648 nm in TPP solutions.[42] Noting that the fluorescence and absorption peak wavelengths of TCPP and TPP are very similar, we anticipate a similar red-shift for TCPP, which corresponds to an energy of ∼0.02 eV. Inclusion of this additional correction gives an overall predicted red-shift of 0.06 eV, which, given the simplicity of our model, represents good agreement with our measured value of 0.084 ± 0.008 eV, and we therefore identify van der Waals-induced deformation as the primary source of the observed shift.

We also highlight an interesting apparent dependence of the fluorescence intensity on the thickness of hBN flakes. The intensity is shown in the inset to Figure 4 as measured for both the green (532 nm) and red (660 nm) excitation laser, and we observe a maximum (minimum) for the green (red) laser for an hBN thickness of ∼100 nm with a variation in intensity of a factor of ∼10. This is a thin film effect arising from the coherent reflection of the excitation laser at the top hBN surface and the Si/SiO_2 interface, highlighting the planarity of the hBN flakes. For a 300 nm SiO_2 thickness, as used here, we would expect constructive interference of incident light when the hBN thickness, t_{BN}, is 106 nm for an exciting wavelength, λ, of 532 nm. For this thickness an enhanced electric field intensity of the incident radiation at the hBN surface is expected, leading to an increase in fluorescence intensity; this value is close to the thickness where the observed maximum occurs. For λ = 660 nm a minimum in intensity is expected for t_{BN} = 104 nm, the thickness where destructive interference is expected. The relevant

equations are included in the SI together with additional results for hBN flakes on a Si substrate without an intentionally grown oxide. These results highlight the highly parallel alignment of the upper and lower hBN interfaces.

CONCLUSIONS

The integration of two-dimensional supramolecular arrays with layered materials and their characterization at the molecular scale offers significant prospects for future research directions. From a fundamental perspective the ability, realized through high-resolution atomic force microscopy, to correlate fluorescence spectra of adsorbed monolayers and submonolayers of organic molecules with specific details of conformation and molecular organization allows a systematic study of the interdependence of structural and optical properties, for example, the "gas-crystal shift",[53] at the microscopic level. In the example considered here, hydrogen bonding is exploited to steer porphyrin dye molecules toward a stable planar arrangement in which their fluorescence spectrum is strongly modified by the substrate and their intermolecular spacing is controlled. Note also that in this configuration the transition dipole moments of the molecules are parallel to the substrate surface, which, combined with the overall two-dimensional assembly, is optimal for interactions with the electromagnetic field of the simple photonic structure formed by the hBN flake.

The hydrogen-bonded network formed by TCPP constitutes a relatively simple supramolecular arrangement, and the demonstration that hBN supports the formation of two-dimensional adlayers deposited from solution and the investigation of their optical properties raise many possibilities for the marriage of the exquisite control of structural organization, which has previously been demonstrated for supramolecular adlayers on conducting surfaces, with the control of fluorescence and its exploitation in chemically responsive optical components. More specifically supramolecular organization can be used to transform local molecular arrangements on surfaces, and thus influence the fluorescence properties through changes in dielectric environment. In addition fluorescence shifts could be used to detect the introduction of guest molecules within supramolecular arrays, providing a readout for engineered molecular recognition processes. In addition, the compatibility of hBN with layered semiconductors and semimetals provides many interesting possible research directions for hybrid nanostructures in which molecular layers are combined with these new materials for exploitation as photonic and sensing devices.

METHODS

The hBN substrates are prepared by exfoliating flakes from single crystals using Scotch tape as previously reported.[54,55] The exfoliated flakes have typical lateral dimensions of 20−100 μm and thicknesses in the range 20−100 nm and are transferred to a SiO_2 surface (a layer of thickness 300 nm grown thermally on a Si substrate) and subsequently cleaned by heating to 350−400 °C in a stream of Ar/H_2 (95:5) for ∼4 h or by flame annealing using a butane torch in a procedure similar to that widely used to prepare Au(111) surfaces. TCPP is synthesized using published procedures,[56] and molecules are deposited on all substrates (hBN, HOPG, and MoS_2) by immersion in solutions of TCPP in either ethanol (EtOH; 13 μM) or dimethylformamide (DMF; 140 μM) for 10−300 s. These relative short immersion times were chosen to avoid the formation of multilayers and substantial coverage with molecules adsorbed in a nonplanar three-dimensional configuration, which occur for longer exposure. All samples were dried in a N_2 stream for about 1 min to remove excess solvent. Fluorescence spectra are acquired using a Horiba LABRAM confocal microscope/spectrometer fitted with two laser sources with wavelengths 532 nm (green) and 660 nm (red) to excite fluorescence. Spectra were acquired from individual flakes using a 50× objective corresponding to spot sizes of 1.1 and 1.7 μm^2 and powers of 4.0 and 1.5 μW for green and red lasers, respectively. In each neutral density filters were used to reduce the incident intensity to the specified level, and the fluorescent radiation was passed through a notch filter matched to the exciting wavelength.

Conflict of Interest: The authors declare no competing financial interest.

Acknowledgment. We gratefully acknowledge the support of Engineering and Physical Sciences Research Council (EP/K01773X/1) for the experimental program, and N.R.C. gratefully acknowledges receipt of a Royal Society Wolfson Merit Award. We are grateful to the University of Nottingham for access to its High Performance Computing facility.

Supporting Information Available: The experimental data on which this paper is based, including image files and spectra, may be found at http://dx.doi.org/10.17639/nott.21. The Supporting Information is available free of charge on the ACS Publications website at DOI: 10.1021/acsnano.5b04443.

Additional details on experimental methodology; details of numerical approach; additional numerical results on adsorption and optical transitions; numerical results for the related molecule tetra(phenyl)porphyrin; additional experimental results showing the fluorescence intensity variation with thickness (PDF)

REFERENCES AND NOTES

1. Barth, J. V.; Costantini, G.; Kern, K. Engineering Atomic and Molecular Nanostructures at Surfaces. *Nature* **2005**, *437*, 671–679.
2. Kudernac, T.; Lei, S.; Elemans, J. A. A. W.; De Feyter, S. Two-Dimensional Supramolecular Self-Assembly: Nanoporous Networks on Surfaces. *Chem. Soc. Rev.* **2009**, *38*, 402–421.
3. Mössinger, D.; Chaudhuri, D.; Kudernac, T.; Lei, S.; De Feyter, S.; Lupton, J. M.; Höger, S. Large All-Hydrocarbon Spoked Wheels of High Symmetry: Modular Synthesis, Photophysical Properties, and Surface Assembly. *J. Am. Chem. Soc.* **2010**, *132*, 1410–1423.
4. Slater, A. G.; Perdigão, L. M. A.; Beton, P. H.; Champness, N. R. Surface-Based Supramolecular Chemistry Using Hydrogen Bonds. *Acc. Chem. Res.* **2014**, *47*, 3417–3427.
5. Stepanow, S.; Lingenfelder, M.; Dmitriev, A.; Spillmann, H.; Delvigne, E.; Lin, N.; Deng, X.; Cai, C.; Barth, J. V.; Kern, K. Steering Molecular Organization and Host-Guest Interactions Using Two-Dimensional Nanoporous Coordination Systems. *Nat. Mater.* **2004**, *3*, 229–233.

6. Nath, K. G.; Ivasenko, O.; Miwa, J. A.; Dang, H.; Wuest, J. D.; Nanci, A.; Perepichka, D. F.; Rosei, F. Rational Modulation of the Periodicity in Linear Hydrogen-Bonded Assemblies of Trimesic Acid on Surfaces. *J. Am. Chem. Soc.* **2006**, *128*, 4212–4213.
7. Furukawa, S.; Tahara, K.; De Schryver, F. C.; Van der Auweraer, M.; Tobe, Y.; De Feyter, S. Structural Transformation of a Two-Dimensional Molecular Network in Response to Selective Guest Inclusion. *Angew. Chem., Int. Ed.* **2007**, *46*, 2831–2834.
8. Kühne, D.; Klappenberger, F.; Decker, R.; Schlickum, U.; Brune, H.; Klyatskaya, S.; Ruben, M.; Barth, J. V. High-Quality 2D Metal-Organic Coordination Network Providing Giant Cavities within Mesoscale Domains. *J. Am. Chem. Soc.* **2009**, *131*, 3881–3883.
9. Griessl, S.; Lackinger, M.; Edelwirth, M.; Hietschold, M.; Heckl, W. M. Self-Assembled Two-Dimensional Molecular Host-Guest Architectures From Trimesic Acid. *Single Mol.* **2002**, *3*, 25–31.
10. Svatek, S. A.; Perdigão, L. M. A.; Stannard, A.; Wieland, M. B.; Kondratuk, D. V.; Anderson, H. L.; O'Shea, J. N.; Beton, P. H. Mechanical Stiffening of Porphyrin Nanorings through Supramolecular Columnar Stacking. *Nano Lett.* **2013**, *13*, 3391–3395.
11. Grill, L.; Dyer, M.; Lafferentz, L.; Persson, M.; Peters, M. V.; Hecht, S. Nano-Architectures by Covalent Assembly of Molecular Building Blocks. *Nat. Nanotechnol.* **2007**, *2*, 687–691.
12. Blunt, M.; Lin, X.; Gimenez-Lopez, M. D. C.; Schröder, M.; Champness, N. R.; Beton, P. H. Directing Two-Dimensional Molecular Crystallization Using Guest Templates. *Chem. Commun.* **2008**, 2304–2306.
13. Theobald, J. A.; Oxtoby, N. S.; Phillips, M. A.; Champness, N. R.; Beton, P. H. Controlling Molecular Deposition and Layer Structure with Supramolecular Surface Assemblies. *Nature* **2003**, *424*, 1029–1031.
14. Karmel, H. J.; Chien, T.; Demers-Carpentier, V.; Garramone, J. J.; Hersam, M. C. Self-Assembled Two-Dimensional Heteromolecular Nanoporous Molecular Arrays on Epitaxial Graphene. *J. Phys. Chem. Lett.* **2014**, *5*, 270–274.
15. Chen, W.; Chen, S.; Qi, D. C.; Gao, X. Y.; Wee, A. T. S. Surface Transfer P-Type Doping of Epitaxial Graphene. *J. Am. Chem. Soc.* **2007**, *129*, 10418–10422.
16. Yokoyama, T.; Yokoyama, S.; Kamikado, T.; Okuno, Y.; Mashiko, S. Selective Assembly on a Surface of Supramolecular Aggregates with Controlled Size and Shape. *Nature* **2001**, *413*, 619–621.
17. Gross, L.; Mohn, F.; Moll, N.; Liljeroth, P.; Meyer, G. The Chemical Structure of a Molecule Resolved by Atomic Force Microscopy. *Science* **2009**, *325*, 1110–1114.
18. Maier, S.; Fendt, L.-A.; Zimmerli, L.; Glatzel, T.; Pfeiffer, O.; Diederich, F.; Meyer, E. Nanoscale Engineering of Molecular Porphyrin Wires on Insulating Surfaces. *Small* **2008**, *4*, 1115–1118.
19. Rahe, P.; Kittelmann, M.; Neff, J. L.; Nimmrich, M.; Reichling, M.; Maass, P.; Kühnle, A. Tuning Molecular Self-Assembly on Bulk Insulator Surfaces by Anchoring of the Organic Building Blocks. *Adv. Mater.* **2013**, *25*, 3948–3956.
20. Burke, S.; Mativetsky, J.; Fostner, S.; Grütter, P. C60 on Alkali Halides: Epitaxy and Morphology Studied by Noncontact AFM. *Phys. Rev. B: Condens. Matter Mater. Phys.* **2007**, *76*, 035419.
21. Zhang, J.; Chen, P.; Yuan, B.; Ji, W.; Cheng, Z.; Qiu, X. Real-Space Identification of Intermolecular Bonding with Atomic Force Microscopy. *Science* **2013**, *342*, 611–614.
22. Sweetman, A. M.; Jarvis, S. P.; Sang, H.; Lekkas, I.; Rahe, P.; Wang, Y.; Wang, J.; Champness, N. R.; Kantorovich, L.; Moriarty, P. Mapping the Force Field of a Hydrogen-Bonded Assembly. *Nat. Commun.* **2014**, *5*, 3931.
23. Korolkov, V. V.; Allen, S.; Roberts, C. J.; Tendler, S. J. B. Green Chemistry Approach to Surface Decoration: Trimesic Acid Self-Assembly on HOPG. *J. Phys. Chem. C* **2012**, *116*, 11519–11525.
24. Korolkov, V. V.; Mullin, N.; Allen, S.; Roberts, C. J.; Hobbs, J. K.; Tendler, S. J. B. The Structure and Formation of Hydrogen-Bonded Molecular Networks on Au(111) Surfaces Revealed by Scanning Tunnelling and Torsional-Tapping Atomic Force Microscopy. *Phys. Chem. Chem. Phys.* **2012**, *14*, 15909.
25. Korolkov, V. V.; Svatek, S. A.; Allen, S.; Roberts, C. J.; Tendler, S. J. B.; Taniguchi, T.; Watanabe, K.; Champness, N. R.; Beton, P. H. Bimolecular Porous Supramolecular Networks Deposited from Solution on Layered Materials: Graphite, Boron Nitride and Molybdenum Disulphide. *Chem. Commun.* **2014**, *50*, 8882–8885.
26. Auwärter, W.; Écija, D.; Klappenberger, F.; Barth, J. V. Porphyrins at Interfaces. *Nat. Chem.* **2015**, *7*, 105–120.
27. Otsuki, J. STM Studies on Porphyrins. *Coord. Chem. Rev.* **2010**, *254*, 2311–2341.
28. Yokoyama, T.; Kamikado, T.; Yokoyama, S.; Mashiko, S. Conformation Selective Assembly of Carboxyphenyl Substituted Porphyrins on Au (111). *J. Chem. Phys.* **2004**, *121*, 11993–11997.
29. Chiang, N.; Jiang, N.; Chulhai, D. V.; Pozzi, E. a.; Hersam, M. C.; Jensen, L.; Seideman, T.; Van Duyne, R. P. Molecular-Resolution Interrogation of a Porphyrin Monolayer by Ultrahigh Vacuum Tip-Enhanced Raman and Fluorescence Spectroscopy. *Nano Lett.* **2015**, *15*, 4114.
30. Goldberg, I. Crystal Engineering of Nanoporous Architectures and Chiral Porphyrin Assemblies. *CrystEngComm* **2008**, *10*, 637.
31. Lipstman, S.; Muniappan, S.; Goldberg, I. Interwoven Hydrogen-Bonded Network Assembly and Supramolecular Isomerism of Meso-5,10,15,20-tetrakis(4-Carboxyphenyl) porphyrin as Its Dimethylformamide Solvate. *Acta Crystallogr., Sect. C: Cryst. Struct. Commun.* **2007**, *63*, o371–o373.
32. MacLeod, J. M.; Ben Chaouch, Z.; Perepichka, D. F.; Rosei, F. Two-Dimensional Self-Assembly of a Symmetry-Reduced Tricarboxylic Acid. *Langmuir* **2013**, *29*, 7318–7324.
33. Berner, S.; Corso, M.; Widmer, R.; Groening, O.; Laskowski, R.; Blaha, P.; Schwarz, K.; Goriachko, A.; Over, H.; Gsell, S.; *et al.* Boron Nitride Nanomesh: Functionality from a Corrugated Monolayer. *Angew. Chem., Int. Ed.* **2007**, *46*, 5115–5119.
34. Pollard, A. J.; Perkins, E. W.; Smith, N. A.; Saywell, A.; Goretzki, G.; Phillips, A. G.; Argent, S. P.; Sachdev, H.; Müller, F.; Hüfner, S.; *et al.* Supramolecular Assemblies Formed on an Epitaxial Graphene Superstructure. *Angew. Chem., Int. Ed.* **2010**, *49*, 1794–1799.
35. Joshi, S.; Bischoff, F.; Koitz, R.; Ecija, D.; Seufert, K.; Seitsonen, A. P.; Hutter, J.; Diller, K.; Urgel, J. I.; Sachdev, H.; *et al.* Control of Molecular Organization and Energy Level Alignment by an Electronically Nanopatterned Boron Nitride Template. *ACS Nano* **2014**, *8*, 430–442.
36. Auwärter, W.; Klappenberger, F.; Weber-Bargioni, A.; Schiffrin, A.; Strunskus, T.; Wöll, C.; Pennec, Y.; Riemann, A.; Barth, J. V. Conformational Adaptation and Selective Adatom Capturing of Tetrapyridyl-Porphyrin Molecules on a Copper (111) Surface. *J. Am. Chem. Soc.* **2007**, *129*, 11279–11285.
37. Buchner, F.; Xiao, J.; Zillner, E.; Chen, M.; Röckert, M.; Ditze, S.; Stark, M.; Steinrück, H. P.; Gottfried, J. M.; Marbach, H. Diffusion, Rotation, and Surface Chemical Bond of Individual 2 H-Tetraphenylporphyrin Molecules on Cu(111). *J. Phys. Chem. C* **2011**, *115*, 24172–24177.
38. Lei, S. B.; Wang, C.; Yin, S. X.; Wang, H. N.; Xi, F.; Liu, H. W.; Xu, B.; Wan, L. J.; Bai, C. L. Surface Stabilized Porphyrin and Phthalocyanine Two-Dimensional Network Connected by Hydrogen Bonds. *J. Phys. Chem. B* **2001**, *105*, 10838–10841.
39. Yuan, Q.; Xing, Y.; Borguet, E. An STM Study of the pH Dependent Redox Activity of a Two-Dimensional Hydrogen Bonding Porphyrin Network at an Electrochemical Interface. *J. Am. Chem. Soc.* **2010**, *132*, 5054–5060.
40. Sundaram, R. S.; Engel, M.; Lombardo, A.; Krupke, R.; Ferrari, A. C.; Avouris, P.; Steiner, M. Electroluminescence in Single Layer MoS_2. *Nano Lett.* **2013**, *13*, 1416–1421.
41. Lopez-Sanchez, O.; Alarcon Llado, E.; Koman, V.; Fontcuberta i Morral, A.; Radenovic, A.; Kis, A. Light Generation and Harvesting in a van Der Waals Heterostructure. *ACS Nano* **2014**, *8*, 3042.

42. Fonda, H. N.; Gilbert, J. V.; Cormier, R. A.; Sprague, J. R.; Kamioka, K.; Connolly, J. S. Spectroscopic, Photophysical, and Redox Properties of Some Meso-Substituted Free-Base Porphyrins. *J. Phys. Chem.* **1993**, *97*, 7024–7033.
43. Khairutdinov, R. F.; Serpone, N. Photoluminescence and Transient Spectroscopy of Free Base Porphyrin Aggregates. *J. Phys. Chem. B* **1999**, *103*, 761–769.
44. DiMagno, S. G.; Wertsching, A. K.; Ross, C. R. Electronic Consequences of Nonplanar Core Conformations in Electron-Deficient Porphyrins: The Structure and Spectroscopic Properties of [5,10,15,20-Tetrakis(heptafluoropropyl)porphinato]cobalt(II). *J. Am. Chem. Soc.* **1995**, *117*, 8279–8280.
45. Bredas, J.-L. Mind the Gap!. *Mater. Horiz.* **2014**, *1*, 17–19.
46. Müller, M.; Langner, A.; Krylova, O.; Le Moal, E.; Sokolowski, M. Fluorescence Spectroscopy of Ultrathin Molecular Organic Films on Surfaces. *Appl. Phys. B: Lasers Opt.* **2011**, *105*, 67–79.
47. Paulheim, A.; Müller, M.; Marquardt, C.; Sokolowski, M. Fluorescence Spectroscopy of PTCDA Molecules on the KCl(100) Surface in the Limit of Low Coverages: Site Selection and Diffusion. *Phys. Chem. Chem. Phys.* **2013**, *15*, 4906–4913.
48. Müller, M.; Le Moal, E.; Scholz, R.; Sokolowski, M. Exciton and Polarization Contributions to Optical Transition Energies in an Epitaxial Organic Monolayer on a Dielectric Substrate. *Phys. Rev. B: Condens. Matter Mater. Phys.* **2011**, *83*, 241203.
49. Müller, M.; Paulheim, A.; Eisfeld, A.; Sokolowski, M. Finite Size Line Broadening and Superradiance of Optical Transitions in Two Dimensional Long-Range Ordered Molecular Aggregates. *J. Chem. Phys.* **2013**, *139*, 044302.
50. Vlaming, S. M.; Eisfeld, A. Tunable Superradiance in Porphyrin Chains on Insulating Surfaces. *J. Phys. D: Appl. Phys.* **2014**, *47*, 305301.
51. Even, U.; Magen, J.; Jortner, J.; Friedman, J.; Levanon, H. Isolated Ultracold Porphyrins in Supersonic Expansions. I. Free-base Tetraphenylporphyrin and Zn-tetraphenylporphyrin. *J. Chem. Phys.* **1982**, *77*, 4374–4383.
52. Riechers, R.; Pentlehner, D.; Slenczka, A. Microsolvation in Superfluid Helium Droplets Studied by the Electronic Spectra of Six Porphyrin Derivatives and One Chlorine Compound. *J. Chem. Phys.* **2013**, *138*, 0–8.
53. Spano, F. C.; Clark, J.; Silva, C.; Friend, R. H. Determining Exciton Coherence from the Photoluminescence Spectral Line Shape in poly(3-Hexylthiophene) Thin Films. *J. Chem. Phys.* **2009**, *130*.074904
54. Dean, C. R.; Young, A. F.; Meric, I.; Lee, C.; Wang, L.; Sorgenfrei, S.; Watanabe, K.; Taniguchi, T.; Kim, P.; Shepard, K. L.; *et al*. Boron Nitride Substrates for High-Quality Graphene Electronics. *Nat. Nanotechnol.* **2010**, *5*, 722–726.
55. Yankowitz, M.; Xue, J.; Cormode, D.; Sanchez-Yamagishi, J. D.; Watanabe, K.; Taniguchi, T.; Jarillo-Herrero, P.; Jacquod, P.; LeRoy, B. J. Emergence of Superlattice Dirac Points in Graphene on Hexagonal Boron Nitride. *Nat. Phys.* **2012**, *8*, 382–386.
56. Daly, D.; Al-Sabi, A.; Kinsella, G. K.; Nolan, K.; Dolly, J. O. Porphyrin Derivatives as Potent and Selective Blockers of Neuronal Kv1 Channels. *Chem. Commun.* **2015**, *51*, 1066–1069.